PERGAMON

International Journal of Heat and Mass Transfer 45 (2002) 571–578

International Journal of HEAT and MASS TRANSFER

www.elsevier.com/locate/ijhmt

Heat transfer and friction coefficients in corrugated ducts confined by sinusoidal and arc curves

J.L. Niu *, L.Z. Zhang

Department of Building Services Engineering, The Hong Kong Polytechnic University, Hung Hom, Kowloon, Hong Kong

Received 4 September 2000; received in revised form 29 April 2001

Abstract

The thermally developing laminar forced-convection flow and heat transfer characteristics in corrugated ducts confined by sinusoidal and arc curves, which are often encountered in honeycomb desiccant wheels, are numerically investigated via the boundary-fitted coordinate system. The control volume-based finite difference technique is applied to obtain the solution utilizing the numerically generated boundary-fitted coordinates. According to this method, the complex domain in the physical plane is transformed into a regular square domain in the computational plane. Studied and graphically illustrated are the effects of aspect ratios and bending ratios of the ducts on the friction coefficients and heat transfer coefficients under uniform wall temperature (**T**) boundary conditions. For the special cases of corrugated ducts such as circular, square, and flat sinusoidal, the results are compared with some findings in the literature, and very good agreement is obtained. Furthermore, variations of the bulk temperature, Nusselt numbers, velocity, and temperature profiles in the entire thermal entry region are plotted.

Keywords: Laminar flow; Corrugated ducts; Friction coefficient; Heat transfer; Boundary-fitted coordinates

1. Introduction

Rotary desiccant wheels are the hearts of various desiccant cooling and dehumidification systems. Therefore, much effort has been devoted to develop wheels of high performance combined with low cost [1,2]. The honeycomb-type wheel, as shown in Fig. 1, has drawn much attention due to its coherent two advantages: large contacting area (3000 m^2/m^3) and compactness [3]. A honeycomb wheel is usually composed of numerous corrugated ducts where process air exchanges moisture and heat with the solid adsorbent. The corrugated sinusoidal duct geometry is the most common in honeycomb wheels because it is advantageous in its simplicity of construction and large surface area. In such small diameter ducts, laminar flow prevails. The cross-sectional geometry of a corrugated sinusoidal duct is shown in Fig. 2. It is observed that the single tube can be approximated with a sine curve for the upper portion and an arc for the lower portion.

Heat transfers of laminar flow have been extensively studied for regularly shaped ducts. The work of Shah and London [4] contains a thorough review of heat transfer under developing and fully developed laminar flow in ducts of many cross-sectional shapes. In recent years, with the progress on computational techniques, ducts of irregular shapes are increasingly investigated. Sherony and Solbrig [5] investigated the heat and mass transfers in a corrugated duct surrounded by a sine curve and a flat plate. Fischer and Martin [6] studied the friction factors in ducts confined by corrugated parallel walls. Ebadian and Zhang [7] studied the fluid flow and heat transfer in a crescent-shaped lumen catheter. Dong and Ebadian [8] provided a numerical analysis of thermally developing flow in elliptic ducts with internal fins. All these studies are informative. However, results for the corrugated sinusoidal ducts (confined by sine and arc curves), which form the honeycomb desiccant wheel being studied, are still not available from the open literature. The authors believe that it is imperative to know the heat and mass transfer characteristics in such ducts,

* Corresponding author. Tel.: +852-2766-7781; fax: +852-2774-6146.

E-mail address: Bejlniu@polyu.edu.hk (J.L. Niu).

0017-9310/02/$ - see front matter
PII: S0017-9310(01)00177-6

Nomenclature

a	half-duct height (m)
A_s	cross-sectional area (m^2)
b	half-duct width (m)
c_p	specific heat (kJ kg^{-1} K^{-1})
D_h	hydraulic diameter (m)
e	bending ratio of duct
f	friction coefficient
h_L	local convective heat transfer coefficient (kW m^{-2} K^{-1})
J	Jacobian operator, Eq. (39)
k	thermal diffusivity (kW m^{-1} K^{-1})
Nu	Nusselt number
Nu_T	Nusselt number for thermally fully developed laminar flow with T condition
P	pressure (Pa)
Pe	perimeter of duct (m)
$\dot{Q}$	heat transfer rate (kW)
Pr	Prandtl number
Re	Reynolds number
T	temperature (K)
u	velocity (m s^{-1})
x, y	dimensional transversal coordinates (m)
z	axial coordinate (m)
R	radius of lower boundary (m)

Greek symbols

α	coefficient, Eq. (34)
β	coefficient, Eq. (35)
γ	coefficient, Eq. (36)
ϕ	coefficient, Eq. (37)
ψ	coefficient, Eq. (38)
τ	aspect ratio
δ	height of lower limit of duct (m)
ξ, η	transversal coordinates in computational plane
μ	dynamic viscosity (kg m^{-1} s^{-1})
ω	angle (rad)
ρ	density (kg m^{-3})
θ	dimensionless temperature

Superscripts and subscripts

$*$	dimensionless
0	for zero bending ratio
b	bulk
i	inlet
L	local
m	mean
w	wall

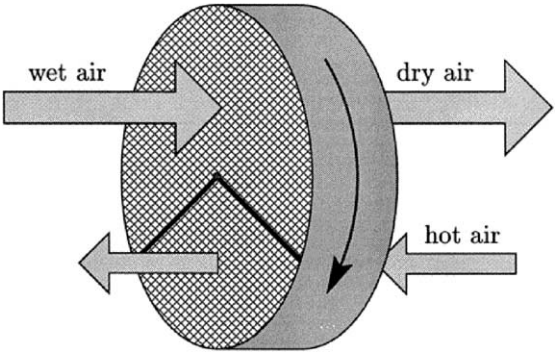

Fig. 1. Configurations of a honeycomb desiccant wheel.

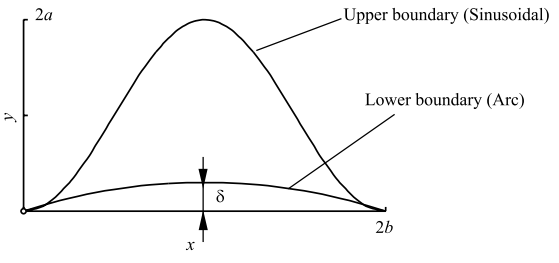

Fig. 2. Cross-sectional view and geometry of a corrugated duct in the wheel.

to further study the adsorption-regeneration dynamics of the wheel.

Owing to the irregular geometry and the small size of the passages, it is very difficult to directly measure anything but overall time–mean performances. The numerical solution method becomes important and will supply the much-needed design information. To address the complexity of the duct geometry, the numerically generated boundary-fitted coordinate system will be applied to discretize the computational domain. According to this technique, the governing equations can be solved with regular geometric methods by transforming the complex duct geometry to a regular square duct.

It should be mentioned now, however, that several other studies have attempted to provide general correlations for ducts of arbitrary cross-sectional shape. Shah [9] used analytical methods to predict overall friction factors and heat transfer. Yilmaz and coworkers provided area- and perimeter-based correlations for friction factors [10] and Nusselt numbers [11]. While the correlations are complicated and reasonably accurate, they do not provide local values around the duct perimeter of heat and momentum transfer. Further, the correlations have only been compared to ducts with regular cross-sections, such as ellipses, rectangles, and triangles.

2. Basic equations

The problem considered here is that of a duct shown in Fig. 2. The upper boundary can be expressed as a sinusoidal function

$$y = a\left[1 - \cos\left(\frac{\pi}{b}x\right)\right], \tag{1}$$

where a is the half-height of the sine duct and b is the half-width of the duct.

The lower boundary is an arc, which can be expressed as:

$$y = R(\sin\omega - 1) + \delta, \tag{2}$$

$$\omega = \arccos\left(\frac{x-b}{R}\right), \tag{3}$$

$$R = \frac{1}{2}\left(\frac{b^2}{\delta} + \delta\right), \tag{4}$$

where R is the radius of the arc (m) and δ is the height of the arc (m). The value of δ can be greater or less than 0. The signs of δ for two consecutive ducts in a wheel are opposite. When $\delta = 0$, the lower boundary becomes a flat plane. This special case was studied by Sherony and Solbrig [5], analytically, which provides a reference for our study.

Aspect ratio of the duct

$$\tau = \frac{a}{b}. \tag{5}$$

Bending ratio of the duct is defined as

$$e = \frac{\delta}{b}. \tag{6}$$

The flow in the duct is considered to be laminar and hydrodynamically fully developed, but thermally developing in the entrance region of the duct. The fluid is Newtonian with constant thermal properties. Additionally, a uniform wall temperature boundary condition is considered.

Momentum equation:

For two-dimensional fully developed laminar flow (fluid has axial velocity only), the Navier–Stokes equations reduce to [12]

$$\mu\left(\frac{\partial^2 u}{\partial x^2} + \frac{\partial^2 u}{\partial y^2}\right) = \frac{\mathrm{d}P}{\mathrm{d}z}, \tag{7}$$

where μ is the dynamic viscosity (Pa s), u is the fluid velocity (m s^{-1}), P is the pressure (Pa), and z is the axial coordinate (m).

Energy equation:

$$\rho c_p u\frac{\partial T}{\partial z} = k\left(\frac{\partial^2 T}{\partial x^2} + \frac{\partial^2 T}{\partial y^2}\right), \tag{8}$$

where T is the fluid temperature (K), k is the thermal diffusivity (kW m^{-1} K^{-1}), ρ is density (kg m^{-3}) and c_p is specific heat of air (kJ kg^{-1} K^{-1}).

The above two equations can be normalized as

$$\frac{\partial^2 u^*}{\partial x^{*2}} + \left(\frac{b}{a}\right)^2\frac{\partial^2 u^*}{\partial y^{*2}} + \frac{4b^2}{D_h^2} = 0 \tag{9}$$

and

$$U\frac{\partial\theta}{\partial z^*} = \frac{\partial^2\theta}{\partial x^{*2}} + \left(\frac{b}{a}\right)^2\frac{\partial^2\theta}{\partial y^{*2}}, \tag{10}$$

where, in the above equations, the dimensionless velocity is

$$u^* = -\frac{\mu u}{(\mathrm{d}P/\mathrm{d}z)D_h^2} \tag{11}$$

and dimensionless temperature is

$$\theta = \frac{T - T_W}{T_i - T_W}, \tag{12}$$

where T_i is the inlet temperature and T_W is the temperature of duct wall.

Dimensionless coordinates:

$$x^* = \frac{x}{2b}, \tag{13}$$

$$y^* = \frac{y}{2a}, \tag{14}$$

$$z^* = \frac{z}{D_h RePr}, \tag{15}$$

where the hydraulic diameter

$$D_h = \frac{4A_s}{Pe}, \tag{16}$$

where A_s is the cross-sectional area of the duct (m^2) and Pe is the perimeter of the duct (m).

In Eq. (10), U is a coefficient defined by

$$U = \frac{u^*}{u_m^*}\frac{4b^2}{D_h^2}, \tag{17}$$

where u_m^* is the average dimensionless velocity on a cross-section and is calculated by

$$u_m^* = \frac{\int\int u^*\,\mathrm{d}A}{A_s}. \tag{18}$$

The characteristics of fluid flow and heat transfer in the duct can be represented by the product of the friction coefficient and the Reynolds number, the dimensionless bulk temperature, and the Nusselt number:

$$(fRe) = \left(-\frac{D_h}{2}\frac{(\mathrm{d}P/\mathrm{d}z)}{\rho u_m^2}\right)\left(\frac{\rho u_m D_h}{\mu}\right) = \frac{1}{2u_m^*}, \tag{19}$$

$$\theta_b(z^*) = \frac{\int\int u^*\theta\,\mathrm{d}A}{\int\int u^*\,\mathrm{d}A}. \tag{20}$$

The local Nusselt number is

$$Nu_{\mathrm{L}} = \frac{h_{\mathrm{L}} D_{\mathrm{h}}}{k}. \tag{21}$$

As will be discussed later, the local Nusselt number decreases asymptotically from a very high value near the entrance of a tube to the fully developed value Nu_{T} at the end of thermal entry length. It can be used to calculate the local convective heat transfer coefficient and to estimate the thermal entry length of a tube.

Considering the energy balance in a control volume of length Δz, heat transferred through convection is

$$\dot{Q}_1 = h_{\mathrm{L}} Pe \Delta z (T_{\mathrm{W}} - T_{\mathrm{b}}). \tag{22}$$

Enthalpy change of the fluid in the control volume is

$$\dot{Q}_2 = \rho u_{\mathrm{m}} A_{\mathrm{s}} c_{\mathrm{p}} \Delta T_{\mathrm{b}}. \tag{23}$$

Since

$$\dot{Q}_1 = \dot{Q}_2 \tag{24}$$

and

$$\Delta z = \Delta z^* D_{\mathrm{h}} RePr = \Delta z^* \frac{\rho c_{\mathrm{p}} u_{\mathrm{m}} D_{\mathrm{h}}^2}{k}, \tag{25}$$

thus

$$h_{\mathrm{L}} = -\frac{1}{4\theta_{\mathrm{b}}} \rho u_{\mathrm{m}} c_{\mathrm{p}} D_{\mathrm{h}} \frac{\Delta \theta_{\mathrm{b}}}{\Delta z} = -\frac{1}{4\theta_{\mathrm{b}}} \frac{k}{D_{\mathrm{h}}} \frac{\Delta \theta_{\mathrm{b}}}{\Delta z^*}. \tag{26}$$

Substituting the above equation to Eq. (21), and considering the control volume to be infinitely small, then we obtain the local Nusselt number as

$$Nu_{\mathrm{L}} = -\frac{1}{4\theta_{\mathrm{b}}} \frac{\mathrm{d}\theta_{\mathrm{b}}}{\mathrm{d}z^*}. \tag{27}$$

The average Nusselt number from 0 to z^* is obtained as

$$Nu_{\mathrm{m}} = \frac{1}{z^*} \int_0^{z^*} Nu_{\mathrm{L}} \, \mathrm{d}z^*. \tag{28}$$

Substituting Eq. (27) to (28), it is obtained that

$$Nu_{\mathrm{m}} = -\frac{1}{4z^*} \ln \theta_{\mathrm{b}}. \tag{29}$$

2.1. Boundary conditions

The flow is assumed hydrodynamically developed and thermodynamically developing. This means that the cross-sectional velocity field does not change with tube length, while the temperature fields vary with tube length. For the honeycomb-type desiccant wheels, strictly speaking, the tube wall is neither an ideal uniform temperature nor an ideal uniform heat flux boundary condition. However, the temperature difference on the wall is relatively small, compared with fluid temperature variations [5]. Therefore, a uniform wall temperature boundary condition (**T**) is considered ($T_{\mathrm{W}} = \mathrm{const}$). In other words

$$u^* = 0, \quad \theta = 0 \text{ on the wall of the duct.} \tag{30}$$

Inlet condition

$$\theta = 1, \quad \text{at } z^* = 0. \tag{31}$$

Another boundary condition often considered is the constant heat flux (**H**) boundary condition. For a heat exchanger with highly conductive materials (e.g., copper, aluminum), the **H** condition may apply. In practice it may be difficult to achieve this boundary condition for non-circular ducts, as discussed in the work of Shah and London [4]. It is already known that Nu_{H} is higher than Nu_{T} for all duct geometries. For sinusoidal ducts, Nu_{H} is approximately 30% higher than Nu_{T}.

3. Results and discussion

3.1. Boundary-fitted coordinates

The difficulty with the complex nature of the duct shape may be circumvented by a numerically generated coordinate system. The transformation between the physical coordinates (x, y) and the boundary-fitted coordinates (ξ, η), which is usually a square domain, is achieved by solving two Poisson equations on the (x, y) domain, see [13,14].

Eqs. (9) and (10) can then be transformed to the computational domain as follows:

$$\frac{\partial}{\partial \xi}\left[\frac{1}{J}\left(\alpha \frac{\partial u^*}{\partial \xi} - \beta \frac{\partial u^*}{\partial \eta}\right)\right] + \frac{\partial}{\partial \eta}\left[\frac{1}{J}\left(\frac{b}{a}\right)^2 \left(\gamma \frac{\partial u^*}{\partial \eta} - \beta \frac{\partial u^*}{\partial \xi}\right)\right] + J \frac{4b^2}{D_{\mathrm{h}}^2} = 0, \tag{32}$$

$$JU \frac{\partial \theta}{\partial z^*} = \frac{\partial}{\partial \xi}\left[\frac{1}{J}\left(\alpha \frac{\partial \theta}{\partial \xi} - \beta \frac{\partial \theta}{\partial \eta}\right)\right] + \frac{\partial}{\partial \eta}\left[\frac{1}{J}\left(\frac{b}{a}\right)^2 \left(\gamma \frac{\partial \theta}{\partial \eta} - \beta \frac{\partial \theta}{\partial \xi}\right)\right], \tag{33}$$

where

$$\alpha = \left[\frac{\partial x}{\partial \eta}\right]^2 + \left[\frac{\partial y}{\partial \eta}\right]^2, \tag{34}$$

$$\beta = \frac{\partial x}{\partial \xi}\frac{\partial x}{\partial \eta} + \frac{\partial y}{\partial \xi}\frac{\partial y}{\partial \eta}, \tag{35}$$

$$\gamma = \left[\frac{\partial x}{\partial \xi}\right]^2 + \left[\frac{\partial y}{\partial \xi}\right]^2 \tag{36}$$

$$\phi = -\left[\frac{\partial x}{\partial \xi}\frac{\partial^2 x}{\partial \xi^2} + \frac{\partial y}{\partial \xi}\frac{\partial^2 y}{\partial \xi^2}\right] \Big/ \left\{\left[\frac{\partial x}{\partial \xi}\right]^2 + \left[\frac{\partial y}{\partial \xi}\right]^2\right\}, \tag{37}$$

$$\psi = -\left[\frac{\partial y}{\partial \eta}\frac{\partial^2 y}{\partial \eta^2}+\frac{\partial x}{\partial \eta}\frac{\partial^2 x}{\partial \eta^2}\right]\Big/\left\{\left[\frac{\partial x}{\partial \eta}\right]^2+\left[\frac{\partial y}{\partial \eta}\right]^2\right\}, \quad (38)$$

$$J = \frac{\partial(x,y)}{\partial(\xi,\eta)} = \frac{\partial x}{\partial \xi}\frac{\partial y}{\partial \eta}-\frac{\partial x}{\partial \eta}\frac{\partial y}{\partial \xi}. \quad (39)$$

Using a control volume-based finite difference procedure [15], the governing differential equations (32) and (33) are reduced to a set of algebraic equation systems. In the process, the non-linear cross-derivative, $\partial^2/\partial\xi\partial\eta$, is relatively small and is treated as a source term. Therefore, iteration is needed to obtain the solution for each equation. Since the equation for the velocity profile does not involve the temperature function, the velocity profile may be determined independently of the temperature profile. In other words, the momentum equation is solved first to find the fully developed velocity field, and then the three-dimensional energy equation with its parabolic properties is solved by ADI techniques [15].

3.2. Validation of the procedure

To assure the accuracy of the results presented, numerical tests were performed for the duct to determine the effects of the grid size. It indicates that 31×31 grids on cross-section and $\Delta z^* = 0.00025$ axially are adequate (less than 0.1% difference compared with 41×41 grids and $\Delta z^* = 0.000125$). For hydrodynamically fully developed laminar flow in ducts, (fRe) is a constant and in the thermal entry region, the local Nusselt number will decrease and approach asymptotically to a lower limiting value Nu_T with the marching of flow. To validate the procedure, (fRe) and Nu_T for some ducts are calculated and compared with the results found in references. The comparisons are listed in Table 1.

From this table, it can be concluded that maximum errors are less than 0.8% for (fRe) and less than 0.9% for Nu_T.

3.3. Effects of bending ratios

For $e = 0$, the corrugated ducts reduce to sine ducts with flat lower boundaries whose results are listed in Table 1. The values of (fRe) and Nu_T are in excellent agreement with the published data. In practical desiccant wheels, e would be greater or less than 0, especially when the ducts are in zones of small diameters. For these ducts, the friction and heat transfer coefficients are affected by the bending ratio e. The effects of e on (fRe) are shown in Fig. 3 and the effects on Nu_T are shown in Fig. 4.

Fig. 3 shows the variations of $(fRe)/(fRe)_0$ (where subscript 0 means $e = 0$) with various e for different aspect ratios. It is seen that the greater the e, the smaller the (fRe). The ratio can be as low as 0.5 when $e = 0.5$ and as high as 1.5 when $e = -0.5$.

Fig. 4 shows the variations of Nu_T/Nu_{T0} (ratio of the Nusselt number for bending duct to that for $e = 0$ with the same aspect ratio) for different aspect ratios. The smaller the bending ratio, the higher the Nusselt number. The comparisons of Figs. 3 and 4 also disclose that the higher the friction coefficients, the higher the Nusselt numbers. Generally speaking, $e > 0$ has positive effects on friction coefficients, but negative effects on Nusselt numbers. On the other hand, $e < 0$ would increase friction coefficients and Nusselt numbers simultaneously, compared to ducts with flat lower

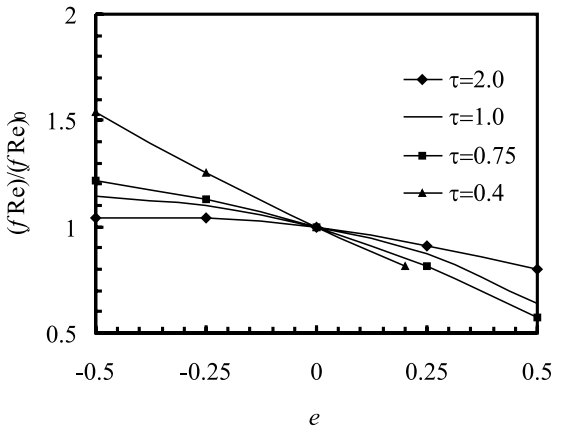

Fig. 3. Effects of duct bending ratios on friction coefficients.

Table 1
Comparisons of (fRe) and Nu_T of fully developed laminar flow for some ducts from the present study and those from the literature

Shape	τ	(fRe)			Nu_T		
		Present study	Refs. [4,5]	Error (%)	Present study	Refs. [4,5]	Error (%)
Circular	1.0	16.081	16	0.51	3.672	3.657	0.41
Square	1.0	14.115	14.227	0.78	3.001	2.976	0.84
Elliptic	0.5	16.941	16.823	0.70	3.766	3.742	0.64
Sine	2.0	14.576	14.553	0.16	2.658	Unavailable	
Sine	1.5	13.934	14.022	0.63	2.614	2.6	0.54
Sine	1.0	12.922	13.023	0.77	2.463	2.45	0.53
Sine	0.75	12.326	12.234	0.75	2.317	2.33	0.56
Sine	0.50	11.173	11.207	0.30	2.135	2.12	0.71

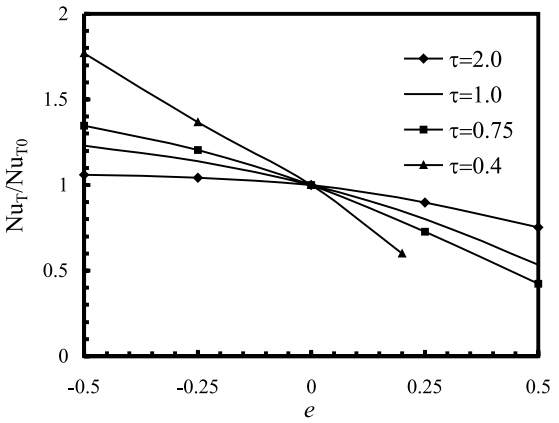

Fig. 4. Effects of duct bending ratios on Nusselt numbers.

boundaries. To know the reason why, let us plot velocity fields in Fig. 5 and temperature fields in Fig. 6. The comparisons of Figs. 5(a) and (b), and 6(a) and (b) show that the bigger the e, the larger the dead spaces in the corners. The larger the dead zones, the more inefficient of the transfer area, which results in decreased friction coefficients and Nusselt numbers. It is interesting to note that the shapes of isotherms and iso-velocities are very similar to those of triangular ducts, however, the maximum velocity and temperature occur closer to the center than those of the triangular ducts [5] for same aspect ratios (duct height-to-width ratio). The shapes of isolines change from triangle with round corners near the boundary to circles at the center gradually. Furthermore, both the velocity gradients and the temperature gradients have their highest values near straight boundaries, while minima are in the corners. These phenomena are also in agreements with the holographic interferometric observations of temperature fields in such ducts [16].

3.4. Local Nusselt numbers

The axial variations of bulk temperature are shown in Fig. 7 for $\tau = 1.0$. Inspection of the curves in this figure reveals that the bulk temperature is strongly variant with e at the entrance region of the duct. However, as the air passes through the duct, the bulk temperature is dependent on the value of e. Positive e results in a bigger bulk temperature than a negative e at the

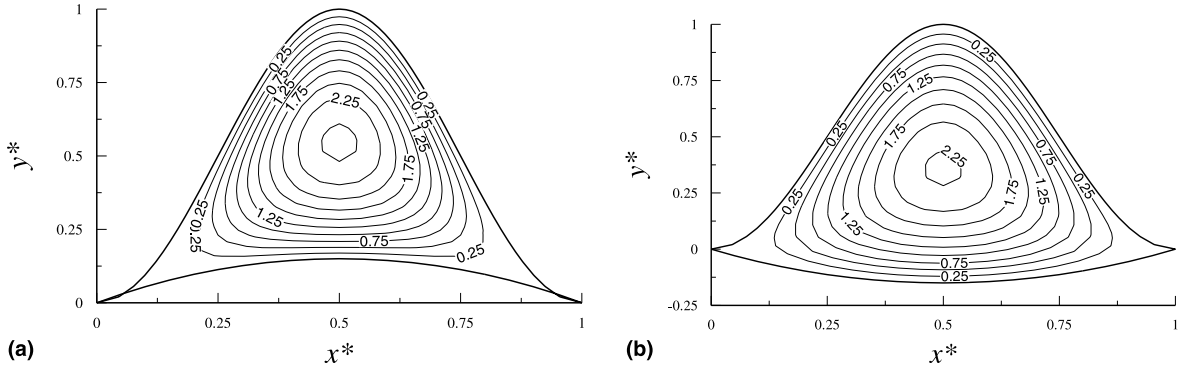

Fig. 5. Fully developed velocity profile, the isoclines are lines of constant u^*/u^*_{m}: (a) $\tau = 0.5$, $e = 0.15$; (b) $\tau = 0.5$, $e = 0.15$.

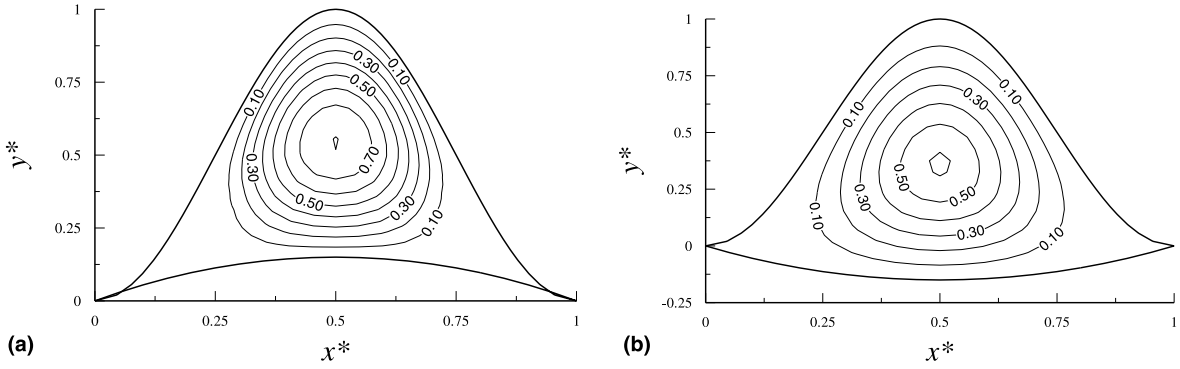

Fig. 6. Isotherms for $\tau = 0.5$ at $z^* = 0.1$: (a) $e = 0.15$; (b) $e = -0.15$. The values are dimensionless temperatures θ.

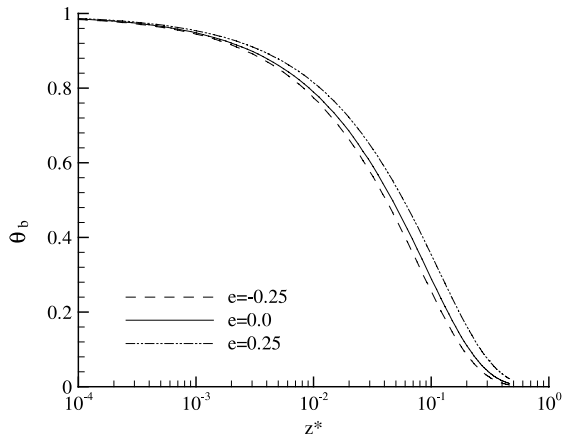

Fig. 7. Axial variations of bulk temperatures, $\tau = 1.0$.

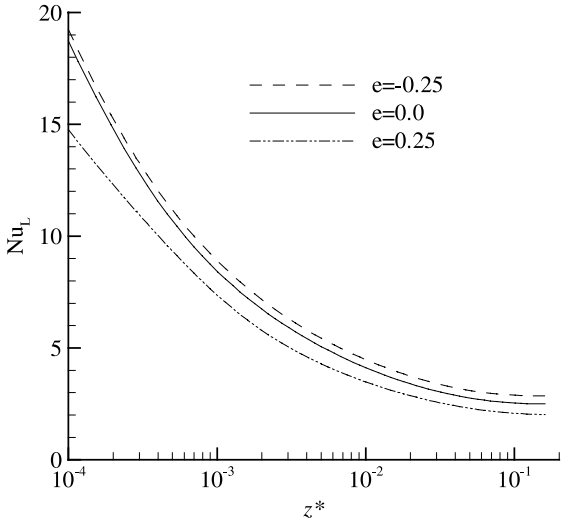

Fig. 8. Axial variations of local Nusselt numbers, $\tau = 1.0$.

same z^* position, suggesting a decreased heat transfer rate. Besides, a bigger bulk temperature would finally lead to a longer thermal entry length.

Local Nusselt numbers against z^* for $\tau = 1.0$ are presented in Fig. 8. It is seen that Nu_L decreases from a high value near the entrance to the fully developed value Nu_T at a greater axial distance, which is presented in Fig. 4. This figure also illustrates that the local Nusselt number decreases dramatically at the entrance region of the duct as the bending ratio increases. However, this variation decreases gradually until it reaches the asymptotic limiting value. Generally speaking, positive e have greater impacts than negative e do. This behavior can also be seen from Fig. 7.

4. Conclusions

Convective heat transfer and fluid flow in corrugated ducts confined by sinusoidal and arc curves are analyzed numerically for various combinations of aspect and bending ratios with uniform wall temperature conditions. The boundary-fitted coordinate is used to solve the difficulty induced by the complex physical domain. The velocity and temperature fields are calculated and graphically illustrated to investigate the effects of sharp corners in the ducts. It is found that bending ratio, e, has a great influence on both the friction coefficients and the Nusselt numbers. The product of friction coefficient and Reynolds number (fRe) could drop by 50% when $e = 0.5$ and rise by 50% when $e = -0.5$, compared to ducts with flat lower boundaries. Positive e would decrease the Nusselt number and negative e would increase the Nusselt number significantly. Besides, bending ratios other than zero could also affects the thermal entry length, local Nusselt numbers, and temperature/velocity profile shapes. All these are due to the fact that the greater the bending ratios, the larger the dead spaces, for both the fluid flow and the heat transfer.

Acknowledgements

This research is funded by the Research Grant Council of the Hong Kong SAR government.

References

[1] W. Jin, A. Kodama, M. Goto, T. Hirose, An adsorptive desiccant cooling using honeycomb rotor dehumidifier, J. Chem. Eng. Jpn. 31 (1998) 706–713.
[2] W. Zheng, W.M. Worek, D. Novosel, Performance optimization of rotary dehumidifiers, ASME J. Solar Energy Eng. 117 (1995) 40–44.
[3] A. Kodama, M. Goto, T. Hirose, T. Kuma, Experimental study of optimal operation for a honeycomb adsorber operated with thermal swing, J. Chem. Eng. Jpn. 26 (1993) 530–535.
[4] R.K. Shah, A.L. London, Laminar Flow Forced Convection in Ducts, Academic Press, New York, 1978.
[5] D.F. Sherony, C.W. Solbrig, Analytical investigation of heat or mass transfer and friction factors in a corrugated duct heat or mass exchanger, Int. J. Heat Mass Transfer 13 (1970) 145–159.
[6] L. Fischer, H. Martin, Friction factors for fully developed laminar flow in ducts confined by corrugated parallel walls, Int. J. Heat Mass Transfer 40 (1997) 635–639.
[7] M.A. Ebadian, H.Y. Zhang, Fluid flow and heat transfer in the crescent-shaped lumen catheter, ASME J. Appl. Mech. 60 (1993) 721–727.

[8] Z.F. Dong, M.A. Ebadian, A numerical analysis of thermally developing flow in elliptic ducts with internal fins, Int. J. Heat Fluid Flow 12 (1991) 166–172.
[9] R.K. Shah, Laminar flow friction and forced convection heat transfer in ducts of arbitrary geometry, Int. J. Heat Mass Transfer 18 (1975) 849–862.
[10] T. Yilmaz, E. Cihan, General equation for heat transfer for laminar flow in ducts of arbitrary cross-sections, Int. J. Heat Mass Transfer 36 (1993) 3265–3270.
[11] T. Yilmaz, General equation for pressure drop for laminar flow in ducts of arbitrary cross-sections, ASME J. Energy Res. Technol. 112 (1990) 220–223.
[12] W.M. Kays, M.E. Crawford, in: Convective Heat and Mass Transfer, McGraw-Hill, New York, 1993, pp. 75–87.
[13] J.F. Thompson, F. Thames, C. Martin, Automatic numerical generation of body-filled curvilinear coordinate system for field containing any number of arbitrary two-dimensional bodies, J. Comput. Phys. 24 (1974) 299–319.
[14] P.D. Thomas, J.F. Middlecoff, Direct control of grid point distribution in meshes generated by elliptic equations, AIAA J. 18 (1982) 652–656.
[15] A.A. Samarskii, P.N. Vabishchevich, Computational Heat Transfer, Wiley, New York, 1995.
[16] R. Tauscher, U. Dinglreiter, B. Durst, F. Mayinger, Transport processes in narrow channels with application to rotary exchangers, Heat Mass Transfer 35 (1999) 123–131.